



UNIVERSITY OF LEEDS

This is a repository copy of *Genetic algorithm-guided discovery of additive combinations that direct quantum dot assembly*.

White Rose Research Online URL for this paper:  
<http://eprints.whiterose.ac.uk/83535/>

Version: Published Version

---

**Article:**

Bawazer, LA, Ihli, J, Comyn, TP et al. (3 more authors) (2015) Genetic algorithm-guided discovery of additive combinations that direct quantum dot assembly. *Advanced Materials*, 27 (2). 223 - 227. ISSN 0935-9648

<https://doi.org/10.1002/adma.201403185>

---

**Reuse**

Unless indicated otherwise, fulltext items are protected by copyright with all rights reserved. The copyright exception in section 29 of the Copyright, Designs and Patents Act 1988 allows the making of a single copy solely for the purpose of non-commercial research or private study within the limits of fair dealing. The publisher or other rights-holder may allow further reproduction and re-use of this version - refer to the White Rose Research Online record for this item. Where records identify the publisher as the copyright holder, users can verify any specific terms of use on the publisher's website.

**Takedown**

If you consider content in White Rose Research Online to be in breach of UK law, please notify us by emailing [eprints@whiterose.ac.uk](mailto:eprints@whiterose.ac.uk) including the URL of the record and the reason for the withdrawal request.



[eprints@whiterose.ac.uk](mailto:eprints@whiterose.ac.uk)  
<https://eprints.whiterose.ac.uk/>

# Genetic Algorithm-Guided Discovery of Additive Combinations That Direct Quantum Dot Assembly

Lukmaan A. Bawazer,\* Johannes Ihli, Timothy P. Comyn, Kevin Critchley, Christopher J. Empson, and Fiona C. Meldrum\*

Biomaterialization, which is the process by which biological organisms form ceramic-based composites, has been widely used as an inspiration for the development of new strategies for materials synthesis.<sup>[1-3]</sup> These bioinspired methods are characterized by mild reaction conditions and promise the ability to generate structures comparable to those found in nature. Central to biogenic control over mineralization is the use of soluble organic additives, where these can even guide the assembly of composite materials<sup>[4-9]</sup> with superior mechanical properties.<sup>[3,4,10]</sup> Many bioinspired mineralization strategies therefore utilize either naturally extracted biomacromolecules or their synthetic analogues,<sup>[1,2,5,7,9,10]</sup> and even small organic species such as amino acids and surfactants can exert considerable control over mineralization, sometimes supporting the formation of complex particle assemblies.<sup>[5,6,8,11-13]</sup> While attractive, however, this approach is still hampered by the difficulty in selecting appropriate organic additives—and in particular combinations of additives—to give materials with target structures and properties. As a result, experiments are often performed on a rather inefficient “trial-and-error” basis.

Due to the complexity of mineralization processes, we are still not in a position to use theoretical methods to predict the soluble additives that will generate materials with specific properties. Experimental strategies are therefore required which enable rapid screening of a potentially vast reaction space. As an elegant approach, DNA-based technologies have been used to evolve libraries of nucleic acids,<sup>[14]</sup> short polypeptides<sup>[15]</sup> and enzymes<sup>[16]</sup> which, when combined with appropriate screening technologies, can be used to identify active biopolymer sequences. However,

these techniques are limited by the requirement for complex enzymatic reactions. As an alternative strategy that bypasses the need for genetic engineering, combinatorial methods can be employed. These can be used to explore tens to hundreds of reaction conditions, where the most promising or “lead” conditions may be selected based on the structures or properties of the resultant material.<sup>[17,18]</sup> Lead conditions can then be used to narrow the reaction landscape in successive screening rounds. Surprisingly, although combinatorial methods are often used in solid-state chemistry to explore, for example, different reagent compositions,<sup>[18]</sup> we are not aware of their use in identifying soluble additives capable of directing mineralization.

In this article we demonstrate how combinatorial methods can be used in conjunction with efficient screening processes to rapidly identify combinations of small organic molecules that are capable of directing the formation of photoluminescent quantum dot minerals in aqueous solution and at room temperature. Indeed, a key feature of biomaterialization processes is that control over mineral formation is achieved using many soluble additives that operate in concert. That this feature has seldom been addressed in bioinspired methods is almost certainly due to the vast number of potential variables, which renders a full, systematic exploration intractable. As a solution to this challenge, we here utilize a genetic algorithm as a bioinspired heuristic that mimics natural evolution. Genetic algorithms use selection, recombination, and mutation strategies to rapidly identify and optimize the combination of conditions (here, soluble additives), which gives rise to materials with target properties.<sup>[19]</sup> Using a pipetting robot to prepare reaction sets and a UV-light table to rapidly assess the reactions for the formation of photoluminescent minerals, we are able to rapidly identify the key additives that promote the formation of quantum dot superstructures from one-pot aqueous reactions.

Our initial library of organic mediators included 23 components, of which 17 were amino acids and 6 were surfactants. Stock solutions of the amino acids were prepared to initial concentrations of  $100 \times 10^{-3}$  M, and explored at concentrations ranging from 0.01 to  $50 \times 10^{-3}$  M, while surfactants were prepared to near their solubility limits in water. Surfactants were included as potential structure-directing agents to drive hierarchical assembly in aqueous solution. The overall screening approach used to identify the key additive set is summarized in **Figure 1**. First, library amino acids and surfactants were randomly mixed in 48 wells of a multi-well plate, such that each well contained between 1–6 amino acids and 1–3 surfactants (**Figure 1A**). Cadmium chloride and thioacetic acid (as a sulfur source)<sup>[20]</sup> were then added to a concentration of  $1 \times 10^{-3}$  M in all wells, as precursors for CdS. After 3 d the plate was viewed under UV illumination (**Figure 1A**) and with a fluorimetric

Dr. L. A. Bawazer,<sup>[†]</sup> J. Ihli, Dr. C. J. Empson,  
Prof. F. C. Meldrum  
School of Chemistry  
University of Leeds  
Leeds, LS1 7HG, UK  
E-mail: bawazer@stanford.edu; F.Meldrum@leeds.ac.uk



Dr. T. P. Comyn  
Institute for Materials Research  
School of Process  
Environmental and Materials Engineering  
University of Leeds  
Leeds, LS1 7HG, UK

Dr. K. Critchley  
School of Physics and Astronomy  
University of Leeds  
Leeds, LS1 7HG, UK

<sup>[†]</sup>Current address: National Institute of Standards and Technology and  
Stanford University, Stanford, CA 94305, USA

This is an open access article under the terms of the Creative Commons  
Attribution License, which permits use, distribution and reproduction in  
any medium, provided the original work is properly cited.

DOI: 10.1002/adma.201403185

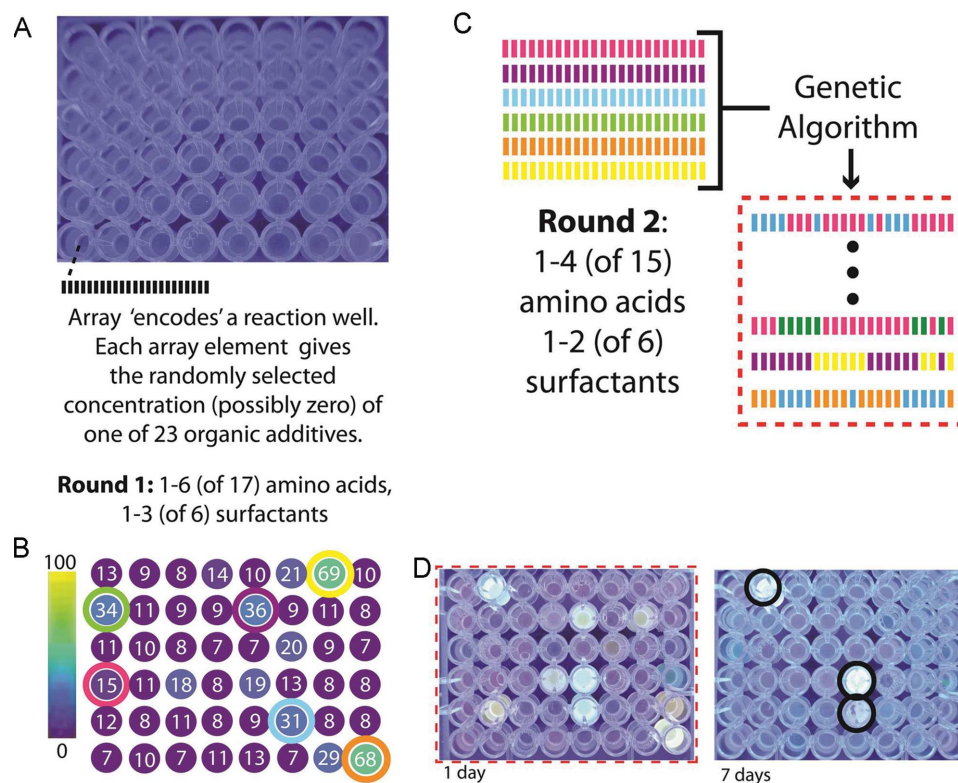


**Figure 1.** Overview of screening rounds 1 and 2. A) Photo of the initial set of 48 CdS aqueous mineralization reaction wells, excited by UV light. Organic additives in each reaction were randomly selected, with selection subject to the "Round 1" constraints indicated. B) Emission intensity from the wells shown in (A), as measured through a band-pass filter centered at 595 nm (excitation at 260 nm). The six highlighted wells were selected as "parent" conditions for genetic algorithm (GA) optimization. C) The GA generates 48 new reaction conditions based on the six parent reactions selected in round 1. D) The 48 CdS mineralization reaction wells (excited by UV light) from round 2 of screening, shown at 1 d and 7 d of reaction, with the winning reactions highlighted in black.

plate-reader (Figure 1B). While no products visibly fluoresced under UV irradiation, six wells with higher emission intensity were identified using a plate-reader, and were selected as "parents." Each parent's reaction parameters, as described by the concentration of each additive in the well, were then input into a genetic algorithm to create pipetting instructions for a new population of 48 combinatorial reactions (Figure 1C).

In the second round, additives were dispensed using the new pipetting instructions, and CdS precursors were added as in round 1. Distinct luminescence was now observed by eye under UV illumination in a number of the wells after 1 d of incubation (Figure 1D, left), demonstrating that the evolution process resulted in increased luminescence. After 7 d, many of the wells lost their distinctive emission (Figure 1D, right), suggesting that either quantum confinement was lost or the surface chemistry of the particles changed (e.g., through ripening or restructuring) as mineralization progressed. However, three reaction conditions maintained their emission properties relative to the rest of the population. Examination of the compositions of these "winning" wells showed that four additives—the amino acids cysteine and aspartic acid, and the surfactants sodium dodecyl sulfate (SDS) and sodium dodecylbenzyl sulfonate (SDBS)—were conserved in each (Figure 2A).

In a final screening round, reactions were prepared such that each well contained each of the four of these conserved

additives (Figure 2B). The majority of the round 3 wells containing surfactant concentrations comparable to those in the round 2 parent wells exhibited intense photoluminescence (Figure 2B, top three rows). The photoluminescence was distinctly reduced in a control subpopulation in which the surfactant concentration range was diluted (Figure 2B, bottom three rows). Just three rounds of screening therefore succeeded in identifying a set of two amino acids and two surfactants that control the formation of fluorescent CdS products. As the final applied selection pressure was the appearance of distinct fluorescence as visible by eye, additional screening rounds would not necessarily be expected to lead to improved fluorescence beyond the applied threshold (i.e., qualitative visibility by eye), but could possibly further refine the concentrations of the reagents required to give this effect.

The morphologies and structures of the products in three of the wells which exhibited the highest photoluminescence in round 3 (Figure 2B, yellow-highlighted wells) were then characterized using transmission electron microscopy (TEM) and electron diffraction. This revealed that CdS nanoparticles  $\approx 2\text{--}5$  nm in size were packed into nanolamellae, which then assembled into meso- (10–100 nm) and micro-scale hierarchical structures of spheres, sheets, and filaments (Figure 3; and Figure S1, Supporting Information). Energy dispersive X-ray spectroscopy (EDX) confirmed that the particle composition was consistent

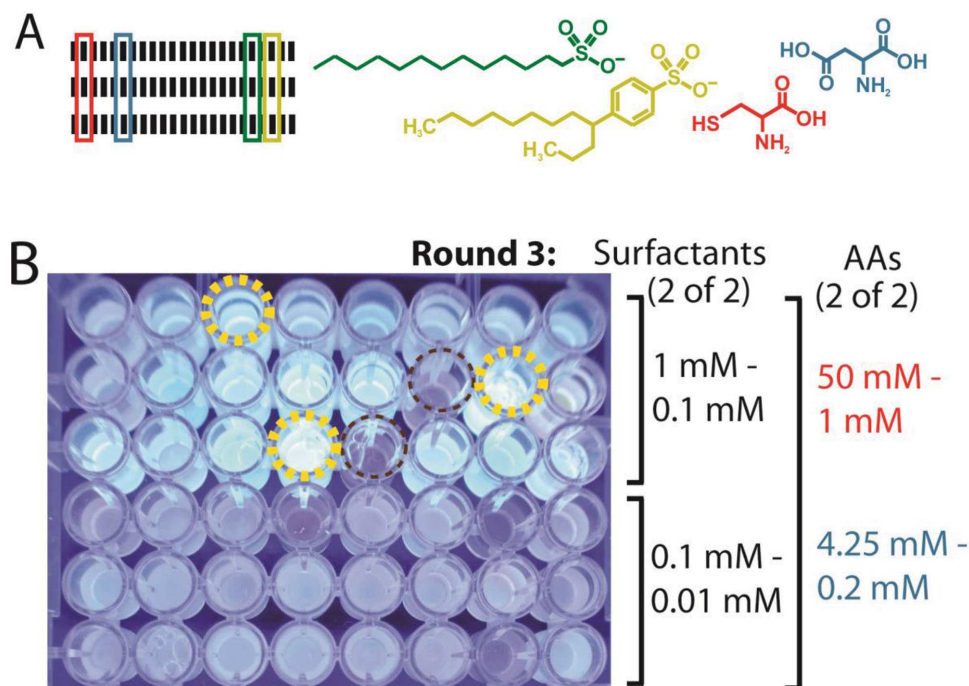


**Figure 2.** Overview of screening round 3. A) Schematic showing that the arrays encoding the three winning reactions from round 2 (Figure 1D, black highlights) share in common the four organic additives shown. B) Photo of 48 CdS mineralization reaction wells from round 3 screening after 7 d (excited by UV light). Round 3 reactions only include the additives shown in (A), with concentrations randomly selected within the ranges indicated. Reaction products from wells showing high photoluminescence (highlighted yellow) and no photoluminescence (highlighted brown) were further characterized.

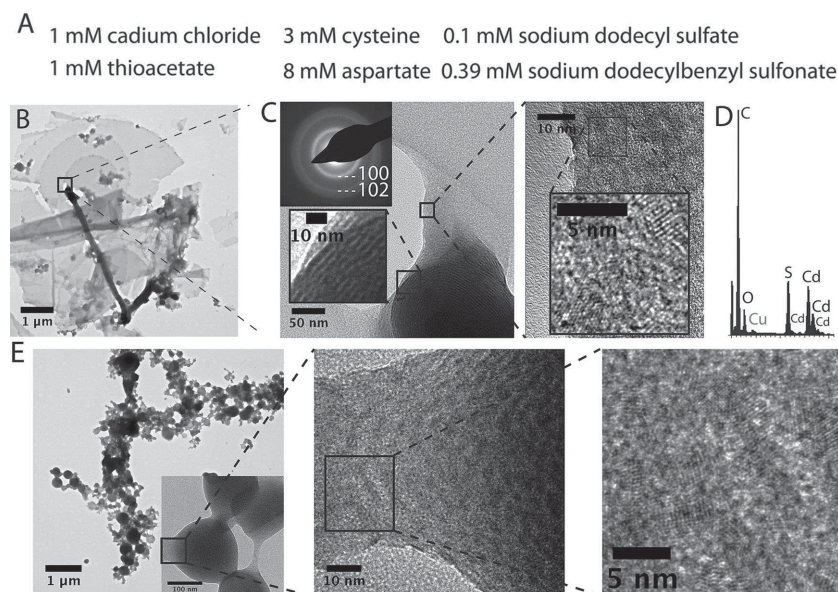


**Figure 3.** EM images of CdS quantum dot superstructures formed in the conditions shown in A) in round 3 of screening (see Figure 2). B) Micron-scale sheet and rod-like structures, C) higher magnification images of the structures shown in (B), revealing nanolamellar, and nanoparticulate subarchitectures. The selected area electron diffraction shows that structures comprise polycrystalline wurtzite-CdS, while D) electron dispersive spectroscopy confirms the presence of cadmium and sulfur. E) Hierarchical rod- and sphere-like structures present found among the mineralization products shown in (A–D).

with CdS (Figure 3), while powder X-ray diffraction (PXRD) of materials produced from scaled up (10 mL) reaction conditions demonstrated the formation of wurtzite (hexagonal) CdS. Typical data from particles generated under the conditions of one of the “winning” wells (“Well 1,”  $3 \times 10^{-3}$  M cysteine,  $8 \times 10^{-3}$  M aspartate,  $0.39 \times 10^{-3}$  M SDBS,  $0.1 \times 10^{-3}$  M SDS,  $1.00 \times 10^{-3}$  M cadmium chloride, and  $1.00 \times 10^{-3}$  M thioacetate) are shown after 1, 4, and 14 d in Figures S2 and S3 (Supporting Information). For comparison, products from two reactions which failed to luminesce in screening round 3 (Figure 2B, brown-highlighted wells) were also characterized. One of these conditions yielded CdS nanoparticles but no hierarchical assembly (Figure S4A, Supporting Information), while the other produced only amorphous materials (Figure S4B, Supporting Information).

The formation of the CdS nanoparticle assemblies formed in Well 1 was also investigated over time. Lamellar nanostructures were observed by TEM (Figure 4A) after 1 d, where these were amorphous by selected area electron diffraction (SAED),

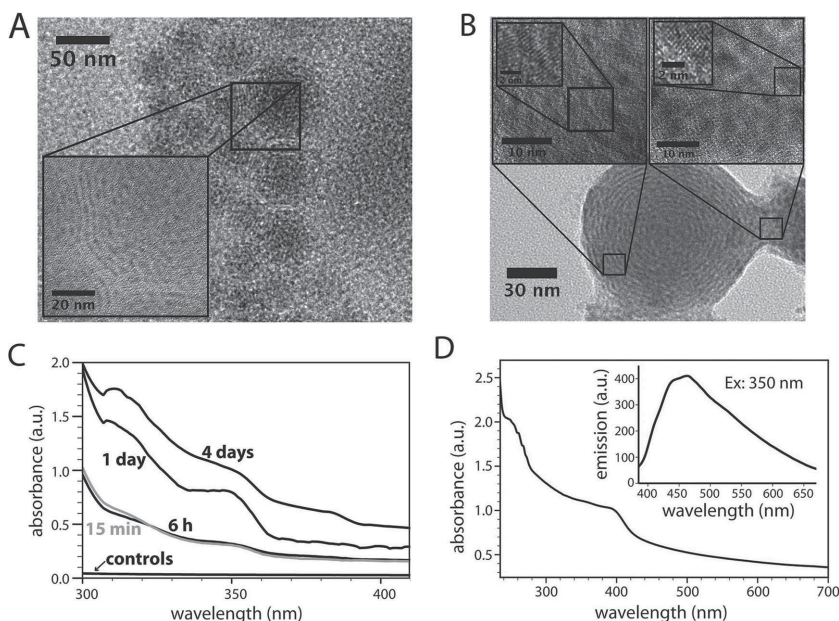


**Figure 4.** Growth of quantum dot superstructures from a “winning” reaction ( $3 \times 10^{-3}$  M cysteine,  $8 \times 10^{-3}$  M aspartate,  $0.39 \times 10^{-3}$  M sodium dodecylbenzyl sulfonate,  $0.1 \times 10^{-3}$  M SDS,  $1.00 \times 10^{-3}$  M cadmium chloride, and  $1.00 \times 10^{-3}$  M thioacetate). A) After 1 d, nanolamella are observed by TEM but crystalline CdS quantum dots are not present. B) After 14 d, TEM reveals distinct CdS nanocrystals within lamella of superstructures. C) UV-vis absorbance over a reaction time-course. Each control is performed in the absence of the sulfur source (thioacetate) and shows no absorbance. D) UV-vis absorbance and photoluminescence (inset) of the structures shown in (B).

and showed very weak and broad diffraction peaks in PXRD (Figure S2, Supporting Information). After 14 d, the composite structures were larger and exhibited more defined lamellae consisting of CdS nanocrystals (Figure 4B; and Figure S3, Supporting Information). UV-vis spectroscopy was also used to study the evolution of these hierarchical composites. Early in the reaction (15 min), an apparent absorption band-edge appeared at  $\approx 365$  nm (Figure 4C), which indicates quantum dot formation. After 1 d, absorbance increased over all wavelengths, while at 4 d, the absorbance continued to increase with the simultaneous emergence of an additional, red-shifted apparent band-edge at  $\approx 380$  nm. UV-vis of the 14 d reaction products showed an apparent band-edge at  $\approx 410$  nm (Figure 4D), which corresponds to an individual particle size of  $\approx 4$  nm.<sup>[21]</sup> The broad emission peak (centered at  $\approx 460$  nm, Figure 4D, inset) of the corresponding photoluminescence spectrum, however, suggests some polydispersity in size. By comparison, a control reaction performed under identical conditions but lacking thioacetate exhibited no absorbance at any stage of the reaction (Figure 4C, “controls”).

The fluorescence behavior of the CdS superstructures also provides valuable insight into the environment of the particles. The emission maximum of  $\approx 460$  nm can be attributed to excitonic fluorescence, which arises from the radiative recombination of thermally detrapped electrons with valence band holes.<sup>[22]</sup> This is typically only observed when hole traps are blocked in an excess of  $\text{Cd}^{2+}$  ions, due to the formation of S-Cd bonds. In aqueous solutions, this is achieved in the presence of both excess cadmium and hydroxide ions, but has also been seen on the formation of nanoparticle assemblies.<sup>[23,24]</sup> The

latter effect appears to be due to a reduction in the degree of hydration of the CdS nanoparticles in these environments, which reduces the number of surface traps, and thus increases the efficiency of the excitonic emission.

Considering then the composition of the “winning” reaction solutions, the efficacy of the four most active additives likely arises from the presence of carboxy, thiol, and sulfonate moieties, which are known to bind effectively to CdS.<sup>[26,27]</sup> At the same time, however, it is not readily apparent why these four additives were collectively conserved to the exclusion of other structurally similar amino acids (such as glutamate). Indeed, a range of different amino acids have previously been shown to serve as capping ligands for CdS, including Arg, Met, Val, Glu, Asp, Gly, His, Pro, Ser, and Trp.<sup>[28–30]</sup> Thus, while the chemical mode by which the four selected additives serve as binding ligands is well established,<sup>[26]</sup> the possibility that they could act in concert to control CdS superstructure formation would have been difficult to predict a priori, without the use of genetic algorithm-based optimization and rapid reaction screening.

The mechanisms by which these nanoparticle assemblies form, and the necessity for the four key additives, are intriguing. Our data show that the surfactant and metal ions initially assemble to form lamellar-type structures (Figure 4A), where this occurs prior to the evolution of highly crystalline CdS. Quantum dot growth then progresses as sulfur is released from thioacetate degradation, where this takes place over several days.<sup>[20]</sup> Growth of the superstructures is then likely to occur by two mechanisms: accretion of the quantum dots onto the existing superstructure templates, and nucleation (and subsequent growth) of CdS quantum dots at the metal sites of the metal-organic scaffolds. This process is consistent with the observed red-shift in the UV-vis absorption (Figure 4C), where this corresponds to the formation of larger quantum dots.<sup>[25]</sup> That the CdS particles grow within a prestructured composite matrix, in an excess of  $\text{Cd}^{2+}$  ions, is also likely to give rise to the observed fluorescence behavior.

Further insight into the relative importance of the four additives in generating the fluorescent quantum dot superstructures was obtained by conducting a series of reactions in which either one or two of the four additives were removed from a “winning” (Figure 3) reaction. All of these new reactions exhibited either no, or reduced ( $<40\%$ ) fluorescence (Figure S5, Supporting Information), and only the sample with all four additives showed fluorescence under UV illumination that was visible to the naked eye. This confirms that all four additives indeed act in concert to generate highly fluorescent CdS products. Interestingly, removal of SDS alone completely eliminated fluorescence (Figure S5, Supporting Information), but some fluorescence was observed under conditions featuring the additional removal of one of the other three additives. Thus, none of the additives are essential to fluorescence, but all contribute

to the fluorescence properties of the “winning” reactions. One possible concerted mode of action might involve specific packing ratios of hydrophobic tails controlling superstructure assembly, while amino acids might cap nascent quantum dots to confine them to sizes amenable to accretion with the pre-existing superstructures. The detailed mechanisms operating in this system are clearly worthy of further study.

The work described here therefore demonstrates that a simple aqueous mixing approach, combined with genetic algorithm optimization heuristics, permits the rapid identification of small, soluble organic molecules that can act in combination to generate fluorescent CdS quantum dot superstructures in a single-pot reaction. We stress that our method is used to rapidly converge on target properties, and thus circumvents the difficulties associated with strategies based on predicting—and then exploiting—complex mineralization mechanisms. Variations of this strategy could incorporate diverse starting chemistries and alternate fitness functions (e.g., by selecting materials with narrow emission spectra) to achieve new aqueous routes toward quantum dot materials for applications in labeling, sensing, and photonics. Beyond quantum dots, this general approach can exploit a vast combinatorial reaction space offered by water-soluble mineralization-mediating additives, and can be directed to the discovery and optimization of new self-assembly mechanisms and “green” synthetic routes to wide range of advanced materials.

## Experimental Section

Prior to each robot dispensing, organic additive stocks were prepared fresh in water (see Supporting Information). Scripts to generate pipetting instructions and perform genetic algorithm optimization were custom written using National Instruments LabVIEW 2011 software (see Supporting Information). A Hamilton MicroLab Star liquid-handling robot was used to prepare combinatorial reactions in 96-well plates (see Supporting Information). After reaction incubation, the multi-well plate was imaged on a UV light table (maximum emission: 305 nm). A Perkin-Elmer EnVision plate reader was used for fluorimetric measurements, using an excitation filter centered at 260 nm (10 nm bandwidth), a dichroic mirror at 315 nm, and an emission filter centered at 595 nm (60 nm bandwidth). After reaction incubation, materials were prepared for TEM or XRD characterization by washing precipitates with water and ethanol by pelleting and centrifugation, and drying them in air on TEM grids or silicon substrates for PXRD analysis (see Supporting Information). For UV-vis and fluorescence spectra shown in Figure 4D, the washed suspension was measured directly in ethanol; while for the UV-vis time-course study (Figure 4C), spectra were acquired directly in reaction solution (see Supporting Information).

## Supporting Information

Supporting Information is available from the Wiley Online Library or from the author.

## Acknowledgements

This work was supported by a UK Engineering and Physical Sciences Leadership Fellowship (FCM and LAB, EP/H005374/1). Electron microscopy was conducted at the Leeds Electron Microscopy and Spectroscopy Centre (LEMAS). The authors thank Rachel Cavill

(Maastricht University) for helpful discussions and Stuart Warriner (University of Leeds) for access to the liquid dispensing robot.

Received: July 16, 2014

Revised: September 12, 2014

Published online:

- [1] F. Nudelman, N. A. J. M. Sommerdijk, *Angew. Chem Int. Ed.* **2012**, *51*, 6582.
- [2] L. A. Bawazer, *MRS Bull.* **2013**, *38*, 509.
- [3] J. Aizenberg, J. C. Weaver, M. S. Thanawala, V. C. Sundar, D. E. Morse, P. Fratzl, *Science* **2005**, *309*, 275.
- [4] J. Seto, Y. Ma, S. A. Davis, F. Meldrum, A. Gourrier, Y.-Y. Kim, U. Schilde, M. Sztucki, M. Burghammer, S. Maltsev, C. Jaeger, H. Coelfen, *Proc. Natl. Acad. Sci. USA* **2012**, *109*, 3699.
- [5] F. C. Meldrum, H. Coelfen, *Chem. Rev.* **2008**, *108*, 4332.
- [6] L. A. Estroff, L. Addadi, S. Weiner, A. D. Hamilton, *Org. Biomol. Chem.* **2004**, *2*, 137.
- [7] A. M. Belcher, X. H. Wu, R. J. Christensen, P. K. Hansma, G. D. Stucky, D. E. Morse, *Nature* **1996**, *381*, 56.
- [8] M. Li, H. Schnablegger, S. Mann, *Nature* **1999**, *402*, 393.
- [9] R. L. Brutchey, D. E. Morse, *Chem. Rev.* **2008**, *108*, 4915.
- [10] Y.-Y. Kim, K. Ganesan, P. Yang, A. N. Kulak, S. Borukhin, S. Pechook, L. Ribeiro, R. Kroeger, S. J. Eichhorn, S. P. Armes, B. Pokroy, F. C. Meldrum, *Nat. Mater.* **2011**, *10*, 890.
- [11] S. Mann, *Nat. Mater.* **2009**, *8*, 781.
- [12] Y. Yin, A. P. Alivisatos, *Nature* **2005**, *437*, 664.
- [13] Y. F. Lu, H. Y. Fan, A. Stump, T. L. Ward, T. Rieker, C. J. Brinker, *Nature* **1999**, *398*, 223.
- [14] L. A. Gugliotti, D. L. Feldheim, B. E. Eaton, *Science* **2004**, *304*, 850.
- [15] S. R. Whaley, D. S. English, E. L. Hu, P. F. Barbara, A. M. Belcher, *Nature* **2000**, *405*, 665.
- [16] L. A. Bawazer, M. Izumi, D. Kolodin, J. R. Neilson, B. Schwenzer, D. E. Morse, *Proc. Natl. Acad. Sci. USA* **2012**, *109*, E1705.
- [17] X. D. Xiang, X. D. Sun, G. Briceno, Y. L. Lou, K. A. Wang, H. Y. Chang, W. G. Wallacefreedman, S. W. Chen, P. G. Schultz, *Science* **1995**, *268*, 1738.
- [18] R. Potyrailo, K. Rajan, K. Stoewe, I. Takeuchi, B. Chisholm, H. Lam, *ACS Comb. Sci.* **2011**, *13*, 579.
- [19] A. K. Sharma, K. H. Son, B. Y. Han, K.-S. Sohn, *Adv. Funct. Mater.* **2010**, *20*, 1750.
- [20] K.awahori, T. Enomoto, H. Furusho, A. Miura, K. Nishio, Y. Mishima, I. Yamashita, *Chem. Mater.* **2007**, *19*, 3105.
- [21] W. W. Yu, L. Qu, Q. Guo, X. Peng, *Chem. Mater.* **2003**, *15*, 2854.
- [22] U. Resch, A. Eychmiller, M. Haase, H. Weller, *Langmuir* **1992**, *8*, 2215.
- [23] N. A. Kotov, F. C. Meldrum, C. Wu, J. H. Fendler, *J. Phys. Chem.* **1994**, *98*, 2735.
- [24] L. Spanhel, M. A. Anderson, *J. Am. Chem. Soc.* **1990**, *112*, 2278.
- [25] B. O. Dabbousi, J. Rodriguez-Viejo, F. V. Mikulec, J. R. Heine, H. Mattoussi, R. Ober, K. F. Jensen, M. G. Bawendi, *J. Phys. Chem. B* **1997**, *101*, 9463.
- [26] I. Medintz, H. Uyeda, E. Goldman, H. Mattoussi, *Nat. Mater.* **2005**, *4*, 435.
- [27] S. S. Narayanan, S. K. Pal, *J. Phys. Chem. B* **2006**, *110*, 24403.
- [28] W. Qiu, M. Xu, X. Yang, Y. Nan, J. Zhang, H. Chen, *J. Alloy Compd.* **2011**, *509*, 8413.
- [29] R. F. Domingos, C. Franco, J. P. Pinheiro, *Environ. Sci. Pollut. R.* **2013**, *20*, 4872.
- [30] Y. Guo, X. Shi, J. Zhang, Q. Fang, L. Yang, F. Dong, K. Wang, *Mater. Lett.* **2012**, *86*, 146.